Energy & Environmental Science

Cite this: *Energy Environ. Sci.*, 2012, **5**, 5694

www.rsc.org/ees

PAPER

A quantitative assessment of the competition between water and anion oxidation at WO_3 photoanodes in acidic aqueous electrolytes

Qixi Mi, Almagul Zhanaidarova, Bruce S. Brunschwig, Harry B. Gray* and Nathan S. Lewis*

Received 19th October 2011, Accepted 7th December 2011
DOI: 10.1039/c2ee02929d

The faradaic efficiency for O_2(g) evolution at thin-film WO_3 photoanodes has been evaluated in a series of acidic aqueous electrolytes. In 1.0 M H_2SO_4, persulfate was the predominant photoelectrochemical oxidation product, and no O_2 was detected unless catalytic quantities of Ag^+(aq) were added to the electrolyte. In contact with 1.0 M $HClO_4$, dissolved O_2 was observed with nearly unity faradaic efficiency, but addition of a hole scavenger, 4-cyanopyridine *N*-oxide, completely suppressed O_2 formation. In 1.0 M HCl, Cl_2(g) was the primary oxidation product. These results indicate that at WO_3 photoanodes, water oxidation is dominated by oxidation of the acid anions in 1.0 M HCl, H_2SO_4, and $HClO_4$, respectively.

1. Introduction

TiO_2 has received intense scrutiny[1–7] as a photoanode material in contact with aqueous electrolytes, both for water oxidation (eqn (1)) and for toxic waste remediation:

$$2H_2O(l) \rightarrow O_2(g) + 4H^+(aq) + 4e^-,\ E^\circ = 1.23\ V\ vs.\ NHE \quad (1)$$

Due to the very positive potentials of the top of the valence band (VB) of metal oxide photoanodes, a prevailing mechanistic hypothesis is that the photoanodic reactions of such electrodes proceed through either free or surface-bound hydroxyl intermediates:[1]

$$H_2O(l) \rightarrow OH\cdot(aq) + H^+(aq) + e^-,\ E^\circ = 2.85\ V \quad (2)$$

Beckman Institute and Kavli Nanoscience Institute, Division of Chemistry and Chemical Engineering, California Institute of Technology, M/C 127-72 1200 E. California Blvd., Pasadena, CA, 91125, USA. E-mail: hbgray@caltech.edu; nslewis@caltech.edu

In strongly alkaline media, in which hydroxide has a high concentration and is the dominant anionic species, hydroxide is presumably readily oxidized by photogenerated holes to produce either free or surface-bound hydroxyl species, leading to the formation of H_2O_2 and eventually to the production of O_2(g) with near unity overall faradaic efficiencies (η). Similar behavior has been observed in alkaline media for metal oxides such as Fe_2O_3,[8–11] which have smaller band gaps than TiO_2 and thus absorb more of the visible region of the solar spectrum. The photoelectrochemical behavior of such systems is consistent with the hypothesis that the valence band of these metal oxides is predominantly O 2p in character, resulting in a similar potential of the valence band edge for all of these metal oxides.[12–14]

In contrast, relatively few studies have elucidated the product distribution of metal oxide photoanodes when operated in acidic or neutral aqueous electrolytes. The reported faradaic efficiencies for O_2(g) evolution, $\eta(O_2)$, at TiO_2/electrolyte interfaces range from 0.09–0.35 in 0.2 M H_2SO_4 under Xe arc lamp illumination[7] to 0.63–0.92 in 0.1–2.0 M NaOH using the 351- and 364-nm emissions of an Ar ion laser.[6] In some cases, low values for $\eta(O_2)$ have been ascribed to the formation and accumulation of H_2O_2

Broader context

Although many chemical fuels can be produced renewably from sunlight, O_2(g) remains the only scalable oxidation product to balance the fuel-forming reactions, and thus the only scalable oxidant to release the chemical energy stored in these fuels. Semiconducting metal oxides (*e.g.*, TiO_2) are known photoanode materials that evolve O_2(g) in contact with aqueous electrolytes under solar illumination. The photoanodic reaction occurs in the absence of an oxygen evolution catalyst, and is generally presumed to involve hydroxyl radicals that are generated by energetic, photoinduced holes in the metal oxide. Herein we demonstrate that acid anions, such as Cl^-(aq), HSO_4^-(aq), and ClO_4^-(aq), that are often considered inert, can be oxidized at WO_3/electrolyte contacts, and effectively compete with water oxidation for the photoinduced holes. The chemical yields of O_2(g) depend not only on the photocurrent, but also on the nature of the electrolyte and on the presence of additives in the electrolyte.

as an intermediate in the four-hole oxidation of two molecules of water to produce one molecule of O_2.[7,15]

WO_3 is an n-type metal oxide semiconductor[16–24] with an indirect band gap of 2.6–2.7 eV,[25] *i.e.*, responsive to the blue end of the visible spectrum ($\lambda \leq 470$ nm). The electron Hall mobility in WO_3 is $\sim$12 $cm^2\ V^{-1}\ s^{-1}$ at room temperature,[26] compared with $\sim$0.3 $cm^2\ V^{-1}\ s^{-1}$ for rutile TiO_2.[27] Extrinsic n-doping is therefore not required for WO_3 to exhibit significant conductivity. Assuming an internal quantum yield of unity for all photons above the 2.6-eV band gap, the theoretically expected photocurrent density (J_{ph}) for WO_3 under 100 mW cm^{-2} of global air mass (AM) 1.5 illumination is 5.0 mA cm^{-2}. Unlike most semiconducting metal oxides (*e.g.*, TiO_2, Fe_2O_3, ZnO), WO_3 is acidic, and thus is resistant to photocorrosion at pH $\leq$ 4,[15] but dissolves in strongly alkaline solutions.

A widely accepted mechanism by which WO_3 (and most other metal oxide photoanodes) produces photocurrent in aqueous electrolytes is that the powerfully oxidizing photogenerated holes, having a potential at the top of the valence band of $\sim$3.0 V *vs.* the normal hydrogen electrode (NHE), generate hydroxyl radicals (eqn (2)).[20,28] According to a computational study,[29] the hydroxyl radical is stabilized on WO_3 surfaces, and the catalytic cycle for O_2(g) evolution is thermodynamically viable at a potential of $\sim$2.3 V *vs.* NHE. Most experimental studies have assumed that either eqn (1) or (2) is responsible for current flow at WO_3 photoanodes in neutral and acidic solutions, as long as the electrolyte is thermodynamically more stable than water at the same pH value. In this work, we have conducted voltammetry, colorimetric assays, and fluorescence-based O_2 detection to quantitatively evaluate the degree of competition between water oxidation (eqn (1) and (2)) and oxidation of other substrates, such as the acid anions of 1.0 M HCl, H_2SO_4, and $HClO_4$, when WO_3 photoanodes are used under acidic conditions. The data indicate that the oxidation of Cl^-(aq), HSO_4^-(aq), or ClO_4^-(aq) in the respective 1.0 M acid dominates the oxidation of water under such conditions, and no O_2(g) is produced directly at WO_3 photoanodes.

2. Experimental

Chemicals

Tungsten powder (Aldrich 510106, ≥99.9%), 1.0 M hydrochloric acid (J. T. Baker 5620), and 4-cyanopyridine *N*-oxide (TCI America C0765, >98%) were used as received. Concentrated sulfuric acid (J. T. Baker 9681, 98%) and perchloric acid (Fisher A2286, 60%) were diluted to 1.0 M using deionized water (18 MΩ·cm resistivity) obtained from a Barnstead Nanopure system. All other chemicals were ACS reagents or higher purity.

Electrochemistry

To form working electrodes, samples of SnO_2:F-coated glass slides (FTO, Hartford Glass, TEC 15) were cut into pieces 1.0 cm in width, and were cleaned with water and ethanol. WO_3 or RuO_2 was then deposited onto the slides. A Ag/AgCl/3.0 M NaCl electrode (Bioanalytical Systems, Inc.) was used as a reference and a Pt mesh was used as the counter electrode. To minimize contamination by NaCl, the reference electrode was isolated from the electrolyte by either a fine glass frit or by a Luggin capillary. All potentials reported herein are relative to the normal hydrogen electrode (NHE), with the Ag/AgCl reference electrode taken to have a potential of $E = 0.209$ V *vs.* NHE. Electrical contact to the working electrode was made either temporarily through a Cu clamp or permanently with Ga–In eutectic. An epoxy adhesive (Loctite Hysol 9460) was utilized for sealing metal leads on the glass slides, but was not used in contact with WO_3 or RuO_2, to avoid oxidation of the epoxy. Voltammetric data were collected at a scan rate of 50 mV s^{-1} with a BAS 100B electrochemical analyzer.

WO_3 photoanodes

A clear, pale yellow solution of peroxytungstic acid (50 mM in W) in 30% (v/v) isopropanol/water[30] was stirred at room temperature for 24–48 h in the presence of a Pt mesh. The Pt mesh and isopropanol reduced the concentration of free H_2O_2 to $\sim$30 ppm (as assessed using EM Quant peroxide test strips), which was required to produce WO_3 films that displayed high photocurrent densities and fill factors. A conductive glass slide was then immersed in the peroxytungstic acid solution to a depth of 1.0 cm, and cathodic electrodeposition was performed, without stirring, at −0.50 V *vs.* Ag/AgCl, using a BAS 100B electrochemical analyzer. Passage of a charge density of −0.25 C cm^{-2} (at a current density of −0.3 mA cm^{-2}) yielded a blue layer of $WO_3 \cdot xH_2O$ on the electrode surface. The sample was then removed from the solution, rinsed with water and ethanol, and dried at 275 °C in air until the blue color had faded completely, typically requiring 5–10 min of drying time. The deposition–dehydration cycle was then repeated. After 3–6 cycles, the electrode was annealed at 500 °C in air for 1 h, yielding a pale yellow film of WO_3 that displayed optical interference patterns to the naked eye. Profilometry (Dektak 3030) indicated that a three-layer WO_3 film had a thickness of $\sim$0.3 μm.

Photoelectrochemistry

Measurements of the photoelectrochemical current density (J) and photoelectrochemical electrolysis data were performed using simulated sunlight obtained from a 150 W Xe arc lamp, a beam collimator, and a global AM 1.5 filter (Oriel). The light intensity at the sample position was adjusted to produce the same photocurrent on a calibrated Si photodiode (Solarex) that would be produced by 100 mW cm^{-2} of global AM 1.5 illumination. The electrolyte, the electrodes, and a magnetic stir bar were positioned in a 25 mL, three-neck round bottom flask that had been fitted with a fused silica window (25 mm in diameter) using an epoxy adhesive (Loctite Hysol 9460). The WO_3 film faced the light source, but the Ag/AgCl reference electrode was not directly exposed to the simulated sunlight. The onset potential of the photoresponse (E_{on}) was estimated at a scan rate of 10 mV s^{-1} using a mechanical shutter (Electro-Optical Products Corp., SH-20) that chopped the simulated sunlight at 0.5 Hz. Bubbling of O_2(g) at 1.0 atm into the electrolyte had no effect on the J–E characteristics of the WO_3 photoelectrodes.

Measurements of dissolved O_2

The O_2 concentration in the anolyte was monitored using a fluorescence-based oxygen sensor (NeoFox, Ocean Optics). An

O_2-sensitive fluorescent patch (HIOXY, Ocean Optics) on the sealed end of a glass tube was separated from the optical fiber inside the glass tube. The oxygen sensor was calibrated against a solution of air-saturated 1.0 M H_2SO_4, which was assumed to have an O_2 solubility of 7.7 mg L^{-1} under 0.21 atm of O_2(g) partial pressure.[31] The Pt counter electrode and the catholyte were housed in another glass tube that was isolated from the anolyte by use of a medium glass frit.

A RuO_2-coated working electrode was prepared by drop-casting a 0.5% (w/v) solution of $RuCl_3 \cdot xH_2O$ in isopropanol onto a conductive glass slide, and calcining at 400 °C in air for 1 h.[32] The working and counter electrodes, as well as the O_2 probe, were then hermetically mounted onto the reaction flask using polytetrafluoroethylene (PTFE) thermometer adapters that had O-ring seals (Ace Glass). The neck that housed the fluorescent probe was wrapped in black tape to block stray light from reaching the sensor. The flask was then filled entirely with Ar-saturated electrolyte (35 ml) and was cooled in a water bath at 20 ± 1 °C. Two-electrode (photo)electrolysis was then performed using a galvanostat (EG&G/PAR 362) interfaced to a computer. The baseline drift in the O_2 concentration was estimated immediately before and after the (photo)electrolysis and was compensated for in each experiment by linear extrapolation.

Measurements of persulfate

Quantitative colorimetry was performed on a UV–visible spectrophotometer (Agilent 8453, 1-cm cuvette). To assay for ozone, a stream of Ar was passed through the anolyte and then into KI (2.00 mL, 2.0 mM in water). The free H_2O_2 concentration was monitored at 410 nm in a mixture of the anolyte (1.00 mL) and titanium(IV) isopropoxide (20 μL of 50 mM solution in isopropanol). Peroxymonosulfate (HSO_5^-) was measured by addition of KI (20 μL, 0.20 M in water) to the anolyte (2.00 mL), followed by measurement of the absorption at 350 or 370 nm within 30 s of mixing. The total peroxy concentration ($[S_2O_8^{2-}] + [HSO_5^-] + [H_2O_2]$) was detected at 470 nm by mixing $[Fe(SCN)_6]^{4-}$ (2.00 mL of 5.0 mM solution in 1.0 M H_2SO_4) and the anolyte (1.00 mL), and stabilizing the reading for 5–10 min. Working curves were established using known concentrations of $Ce(SO_4)_2$(aq) or H_2O_2.

Microscopy and X-ray diffraction (XRD)

Field emission scanning electron micrography was performed on a Zeiss model 1550VP, and XRD data were collected with a PANalytical X'Pert using Cu-Kα excitation.

3. Results

Thin-film WO_3 photoanodes

Fig. 1 shows a micrograph and an XRD pattern of a typical thin-film WO_3 photoanode. Annealing at 500 °C converted amorphous $WO_3 \cdot xH_2O$ into WO_3 crystallites ~50 nm in size. As shown in Fig. 1b, bulk monoclinic WO_3 in the $P2_1/n$ space group[33] exhibits a powder XRD pattern that has systematically absent or attenuated (hkl) peaks, where at least one of h, k, and l is an odd number. However, the electrodeposited WO_3 thin films exhibited a further simplified XRD pattern, where only the (00l),

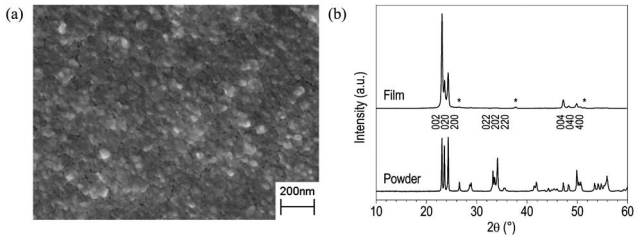

Fig. 1 (a) Scanning electron micrograph and (b, top) X-ray diffraction pattern of a typical WO_3 thin film electrodeposited on conductive glass. Diffraction peaks due to the SnO_2:F (FTO) coating are labeled by asterisks. (b, bottom) XRD of powdered WO_3 with indices is included for comparison.

(0k0), and (h00) peaks (h, k, and l are even numbers) were observed, indicating that the (002), (020), or (200) crystallographic plane of the WO_3 crystallites was oriented nearly parallel to the glass substrate over a macroscopic area. The WO_3 crystallites were preferentially exposed through the (002) face, as evidenced by the fact that the (002) peak displayed the highest intensity.[34]

The WO_3 films produced by cathodic electrodeposition from peroxytungstic acid solutions were transparent, smooth, and adhered well to the conductive glass substrate. The as-deposited $WO_3 \cdot xH_2O$ was an amorphous gel that was dark blue in color and was electrically conductive, both presumably due to the presence of free electrons in the film. The conductivity allowed for a relatively constant film growth rate. Upon dehydration, the volume of the $WO_3 \cdot xH_2O$ film decreased significantly, producing cracks and peeling of the film.[30] This behavior was mitigated by repeated deposition and dehydration, because the small cracks that formed during a previous step of dehydration mended in a subsequent deposition step.

Cyclic voltammetry in acids

Fig. 2 depicts the cyclic voltammetric behavior observed for WO_3 photoanodes in contact with a series of strong aqueous acids. As shown in Fig. 2a, in 1.0 M H_2SO_4 under room light, referred to as "dark", the WO_3 films produced small, capacitive current densities (<40 μA cm^{-2}) for potentials up to 2.0 V *vs.* NHE. The photocurrent became significant (≥1 μA cm^{-2}) at E_{on} = 0.43 V

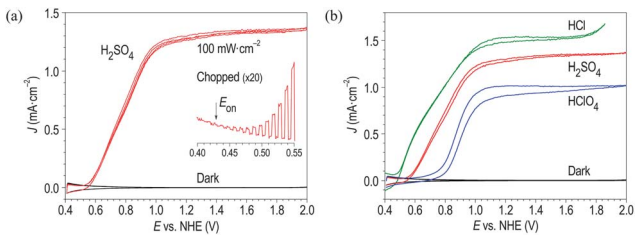

Fig. 2 Cyclic voltammograms of WO_3 photoanodes in contact with 1.0 M aqueous strong acids. Conditions: (a) In 1.0 M H_2SO_4, under continuous or chopped simulated sunlight (global AM 1.5 illumination, 100 mW cm^{-2}). The onset potential of photocurrent (E_{on}) is indictaed by an arrow. (b) WO_3 in 1.0 M HCl (green), H_2SO_4 (red), and $HClO_4$ (blue), under simulated sunlight. Both panels also depict the results from control experiments in 1.0 M H_2SO_4 in the dark (black).

vs. NHE and reached a plateau value (J_{ph}) at 1.0 V *vs.* NHE. Values of $J_{ph} > 6$ mA cm^{-2} were recorded when the incident light intensity was increased beyond 100 mW cm^{-2}.

Fig. 2b compares the *J*–*E* behavior observed for WO_3 in contact with 1.0 M HCl, H_2SO_4, and $HClO_4$, respectively. After *J*–*E* measurements under illumination in 1.0 M HCl, the WO_3 photoanode exhibited a strong odor, and the Cu clamp in the headspace developed a blue-colored rust, both of which indicated the production of Cl_2(g). In contact with 1.0 M $HClO_4$, the WO_3 photocurrent was not as stable as in contact with 1.0 M HCl or 1.0 M H_2SO_4, and a moderate decrease was detected between the forward and backward segments of a single scanning cycle. However, the performance of the electrode in 1.0 M $HClO_4$ recovered fully after rinsing with water and drying in air, and the optical interference pattern of the WO_3 thin film remained unchanged.

Fig. 3 depicts the effect of addition of 0.20 M 4-cyanopyridine *N*-oxide (CPO) on the *J*–*E* behavior of the WO_3/1.0 M $HClO_4$ contact. CPO is a) not basic in character, having a conjugate p$K_a = -0.73$;[35] b) chemically stable under such conditions in the dark, showing an irreversible oxidation at 2.51 V *vs.* NHE in CH_3CN;[36] and c) transparent to visible light. Relative to the *J*–*E* behavior depicted in 1.0 M $HClO_4$ in Fig. 2b, addition of CPO produced stable photoelectrochemical behavior at the WO_3/1.0 M $HClO_4$ interface, and yielded a negative shift of 0.20 V in E_{on}, as well as a 35% increase in J_{ph} at 100 mW cm^{-2} of simulated global AM 1.5 illumination.

Yields of dissolved O_2

A fluorescent-type probe was used to determine $\eta(O_2)$ for WO_3 electrodes under a series of acidic conditions during galvanostatic (photo)electrolysis for 1000 s at a current of 1.00 mA and a current density of 1 mA cm^{-2}. A RuO_2 electrode (in the dark), also at a constant anodic current of 1.00 mA and a current density of 1 mA cm^{-2}, served as a control electrode for the production of O_2.[32] In separate three-electrode galvanostatic (photo)electrolysis experiments, which employed a Ag/AgCl reference electrode but not the O_2 probe, the working electrode potential was 0.9–1.2 V *vs.* NHE for illuminated WO_3 photoanodes, and was 1.5–1.6 V *vs.* NHE for RuO_2 in the dark (Fig. 4).

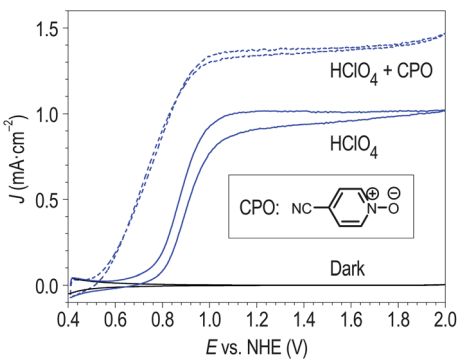

Fig. 3 Cyclic voltammograms (dashed) of WO_3 photoanodes in 1.0 M $HClO_4$ with 0.20 M 4-cyanopyridine *N*-oxide (CPO, inset), under 100 mW cm^{-2} global AM 1.5 illumination. Control experiments in the absence of CPO or in the dark are also shown (solid lines).

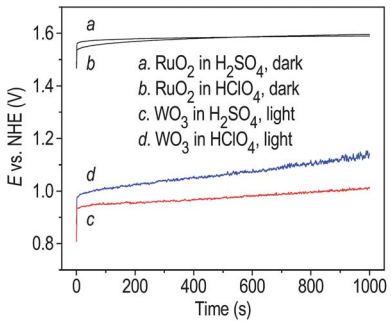

Fig. 4 The electrode potentials of a dark RuO_2 electrode and of illuminated WO_3 photoanodes during galvanostatic (photo)electrolysis (1.00 mA, 1000 s). Two electrolytes, 1.0 M H_2SO_4 and 1.0 M $HClO_4$, were tested for each type of working electrode.

Fig. 5 shows that the RuO_2 electrode displayed an O_2 yield in close accord with the theoretically expected 83 μg of O_2 produced after passage of 1.00 C of anodic faradaic charge. The heterogeneous nature of the electrocatalysis was confirmed by the observation of O_2 bubbles clinging to the RuO_2 surface, even while stirring and under conditions at which the measured concentration of dissolved O_2 was much lower than its solubility. The slightly lower $\eta(O_2)$ in 1.0 M $HClO_4$ relative to that observed in 1.0 M H_2SO_4 could result from a systematic error, because the O_2 sensor was calibrated against 1.0 M H_2SO_4.

The observed electrolysis products depended on the electrolyte and on the presence of additives in the solution. In pure 1.0 M H_2SO_4, no bubbles were observed on the WO_3 photoanode, and the change in the O_2 concentration was below the detection limit (0.02 ppm) of the fluorescent probe. When 0.050 mM Ag_2SO_4 was added as a catalyst to the 1.0 M H_2SO_4, the $\eta(O_2)$ increased to ~0.82. In a separate experiment, after photoelectrolyzing air-saturated 1.0 M H_2SO_4 with 0.050 mM Ag_2SO_4, gas bubbles were visible on the walls of the flask and on the edges of the WO_3 photoanode, but not on the WO_3 surface. In contrast, in 1.0 M $HClO_4$, WO_3 under illumination produced O_2 that was comparable with the amount produced by RuO_2 in the dark. However, although bubbles were observed on the RuO_2 electrode, no gas bubbles were observed on WO_3 electrodes in 1.0 M $HClO_4$. The addition of 0.10 M CPO to 1.0 M $HClO_4$ led to an undetectable O_2 yield, and the anolye turned pale brown after

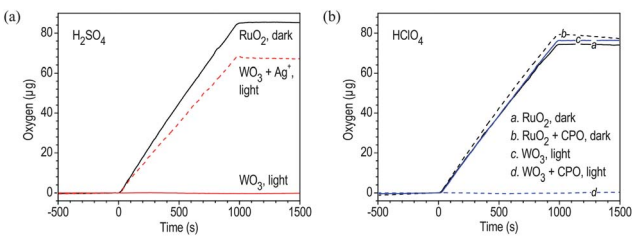

Fig. 5 Production of dissolved O_2 during photoelectrolysis of (a) 1.0 M H_2SO_4 and (b) 1.0 M $HClO_4$ at constant currents (1.00 mA, 1000 s). A RuO_2 electrode (black) yielded O_2 at faradaic efficiencies near unity in the dark, whereas the products formed at illuminated WO_3 photoanodes depended on the electrolyte (red or blue) and the additive (dashed): 0.050 mM Ag_2SO_4 or 0.10 M 4-cyanopyridine *N*-oxide (CPO).

photoelectrolysis. The O_2 yield was not measured in 1.0 M HCl, because the fluorescent probe was not compatible with Cl_2.

Persulfate formation

Aliquots of the anolyte were withdrawn for colorimetric analyses after photoelectrolysis (1000 s at 1.00 mA) of air-saturated 1.0 M H_2SO_4 (24 ml) using a WO_3 photoanode. The concentration of ozone was below the detection limit (1 ppm) of KI. The concentration of free H_2O_2 was below the detection limit (0.1 ppm) of Ti (IV). The total persulfate ($S_2O_8^{2-}$ + HSO_5^-) concentration was determined, in two runs, to be 4.42 ± 0.05 μmol, corresponding to an η of 0.85 ± 0.01, which included a small contribution (0.05) from HSO_5^-(aq). A control experiment indicated that ~10% of $S_2O_8^{2-}$(aq) in 1.0 M H_2SO_4 was hydrolyzed, producing HSO_5^-(aq) after 1 day at room temperature.

4. Discussion

Competition between water and anion oxidation

The data and observations reported herein indicate that for WO_3 photoanodes operated in acidic aqueous electrolytes under simulated solar illumination, O_2 was either not formed at all or was a secondary oxidation product. When high values of $\eta(O_2)$ were observed, the O_2 bubbles were not localized on the electrode surface, in contrast to the case for the electrocatalytic oxidation of water to O_2(g) effected by RuO_2 electrode surfaces. The interference pattern of WO_3 thin films remained identical to the naked eye after multiple experiments, which suggests that substantial photocorrosion of WO_3 photoanodes did not occur in 1.0 M H_2SO_4.

The absence of direct O_2 production indicates that other reductants effectively kinetically competed with water oxidation (eqn (1) and (2) for capture of photogenerated holes at WO_3 photoanodes under acidic conditions. The oxidation of Cl^- to Cl_2 ($E^\circ = 1.36$ V) in acidic and neutral water is a key step in the chloralkali process. The same reaction has been shown[15] to be driven by light at WO_3 photoanodes in contact with 1.0 M HCl. This hypothesis is consistent with the indications of Cl_2(g) production for WO_3/1.0 M HCl contacts.

In H_2SO_4 solutions, an analogous anion-derived hole-transfer process occurs at a Pt anode in the dark,

$$2HSO_4^-(aq) \rightarrow S_2O_8^{2-}(aq) + 2H^+ + 2e^-,\ E^\circ = 2.12\ V \quad (3)$$

with $\eta(S_2O_8^{2-})$ up to 0.90.[37] The observations described herein indicate that eqn (3) dominated the oxidative processes at WO_3 photoanodes in 1.0 M H_2SO_4, where $S_2O_8^{2-}$(aq) and its hydrolysis product HSO_5^-(aq), instead of O_2(g), were the only detectable photoelectrochemical products. A prior study[15] reported that considerable amounts of O_2(g) were collected after 4 h of unfiltered Hg lamp irradiation of WO_3 anodes in 0.5 M H_2SO_4, but this observation can be attributed to photodegradation of $S_2O_8^{2-}$(aq), because $S_2O_8^{2-}$(aq) strongly absorbs at 254 nm.[38]

In 1.0 M $HClO_4$, the perchlorate radical could initially be formed,

$$ClO_4^-(aq) \rightarrow ClO_4\cdot(aq) + e^-,\ E^\circ = 2.75\ V \quad (4)$$

as has been identified in nonaqueous electrochemistry.[39,40] In aqueous solutions, the $ClO_4\cdot$ radical does not form stable peroxy species, and yields O_2 as a final oxidation product. The temporary decrease in photocurrents during the operation of WO_3 in 1.0 M $HClO_4$ could be due to weak binding of $ClO_4\cdot$ to active sites on the WO_3 surface. This behavior thus agrees with the observations that high values of $\eta(O_2)$ were obtained during the operation of WO_3 as a photoanode in 1.0 M $HClO_4$, but the O_2 was produced homogeneously in the solution and not primarily at the solid/liquid interface.

The distinct cyclic voltammograms (Fig. 2b) observed in 1.0 M HCl, H_2SO_4, and $HClO_4$, respectively, provide additional evidence that the current-limiting process at the WO_3 photoanode involved reactions with the anions of these electrolytes (Fig. 6) as opposed to direct oxidation of water. The value of E_{on} is affected by the semiconductor properties of WO_3 as well as by the redox potential of the electrolyte,[41] so the variation of E_{on} in these acids cannot be simply estimated from the E° values for oxidation of the acid anion. E_{on} also depends on the solution pH, due to protonation of the WO_3 surface.[42]

Although H_3PO_4 solutions were not evaluated in our work, in view of the low acidity of phosphoric acid, the stable peroxydiphosphate ($P_2O_8^{4-}$) species, instead of O_2(g), would be expected to be formed at illuminated WO_3/H_3PO_4 interfaces.

Effect of additives

The final product distribution can of course be modified by additives that can catalyze secondary reactions in the solution (Fig. 5). For example, Ag^+ is a facile two-electron redox catalyst that regenerates HSO_4^-(aq) from $S_2O_8^{2-}$(aq), with concomitant evolution of O_2:[43]

$$Ag^+(aq) \rightarrow Ag^{3+}(aq) + 2e^-,\ E^\circ = 1.9\ V \quad (5)$$

$$2Ag^{3+}(aq) + 2H_2O(l) \rightarrow 2Ag^+(aq) + O_2(g) + 4H^+(aq) \quad (6)$$

In 1.0 M H_2SO_4 solutions, SO_4^{2-} coordinates Ag^+ and Ag^{3+} at low concentrations, and no cathodic current due to the electroplating of Ag(s) on WO_3 occurred in the dark. The above reaction scheme is fully consistent with the detection of high $\eta(O_2)$ in 1.0 M H_2SO_4 solutions that contained Ag^+, while no O_2 was detected during the photoelectrolysis of pure 1.0 M H_2SO_4.

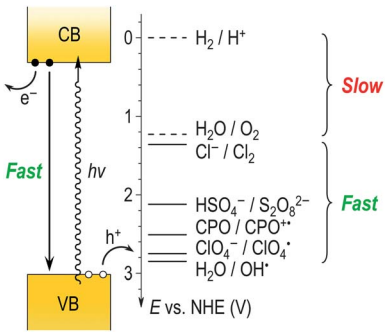

Fig. 6 Redox couples accessible to photogenerated holes in the valence band (VB) of WO_3. The reactions that involve the H_2/H^+ and H_2O/O_2 couples have very slow rates in the absence of a catalyst.

A useful probe molecule is 4-cyanopyridine *N*-oxide (CPO), which can act as a scavenger for energetic holes but is not a sacrificial reagent:

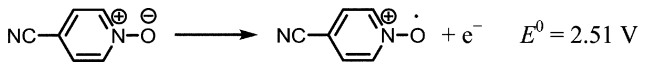

(7)

Because of its relatively positive oxidation potential, CPO did not interfere with O_2(g) evolution at a RuO_2 electrode in 1.0 M $HClO_4$, and O_2(g) was evolved at 1.5–1.6 V *vs.* NHE (Fig. 4). However, on WO_3 photoanodes, oxidation of CPO effectively competed with the oxidation of water or ClO_4^-, substantially enhancing the apparent *J*–*E* performance (Fig. 3). The chemical energy stored in $CPO^{+}\cdot$, however, results in decomposition of $CPO^{+}\cdot$ rather than in the oxidation of water to O_2(g).

Photoanode efficiencies

The energy-conversion efficiency of a photoanode oxidizing a reduced species, A^-, to produce an oxidized species, A, that could in turn be reversibly converted back to A^- by reduction at an ideally nonpolarizable electrode, in a regenerative cell configuration, is given by:

$$\text{Efficiency} = \frac{J[E(\text{A}/\text{A}^-) - E]}{P_{\text{in}}} \quad (8)$$

where P_{in} is the illumination power density, *J* is the photocurrent density, *E* is the applied photoanode potential, and $E(A/A^-)$ is the redox potential of the species being oxidized. Instead, when a chemical product is made at the photoanode, $E(A/A^-)$ is the redox potential at which the chemical product would be produced at an ideally nonpolarizeable, kinetically reversible anode in the dark.

Clearly, for a specific *J*–*E* behavior of the photoanode *vs.* a fixed reference electrode, the calculated energy-conversion efficiency of the photoelectrode will depend critically upon the value of $E(A/A^-)$. For example, if O_2(g) is produced by a photoanode, the relevant value of $E(O_2/H_2O)$ in eqn (8) under standard conditions is 1.23 V *vs.* NHE, whereas if a species with a more positive redox potential (*e.g.*, persulfate) is produced, the identical photoanodic *J*–*E* behavior would in fact correspond to a higher efficiency for the photoanode. This situation occurs because persulfate has a much more positive potential, $E^\circ(S_2O_8^{2-}/HSO_4^-) = 2.12$ V, and is much more oxidizing than O_2, so more energy is stored chemically by production of persulfate than by production of O_2. Of course, realization of the full energy content of the oxidized product would require either a reversible chemical reaction, or a fuel cell operating at the reversible potential for producing the reduced species A^- from the oxidized species A that was produced by oxidation at the photoanode.

For WO_3 photoanodes in contact with 1.0 M HCl, H_2SO_4, and $HClO_4$, the predominant oxidation products are Cl_2(g), $S_2O_8^{2-}$(aq), and O_2(g), so E° = 1.36, 2.12, and 1.23 V, respectively. These values would therefore represent the relevant redox potentials to use in eqn (8) to calculate the efficiency for WO_3 photoanodes in each case under standard conditions. Fig. 7 plots the efficiency-potential characteristics of WO_3 in contact with 1.0 M H_2SO_4, calculated using two possible values of E°, 2.12 or 1.23 V, in eqn (8). The assumption that O_2(g) is the anodic product and that $E^\circ = 1.23$ V at the WO_3/1.0 M H_2SO_4 interface would lead to an underestimation of the efficiency, and would produce a maximum efficiency of 0.34% at $E = 0.90$ V. Instead, adopting $E^\circ = 2.12$ V yields a maximum efficiency of 1.3% at $E =$ 1.00 V. Note that this maximum value represents a lower limit of the internal efficiency of the WO_3/1.0 M H_2SO_4 contact, because the WO_3 thin films used in this study were not optically dense and thus did not absorb all of the incident photons above the 2.6-eV band gap.

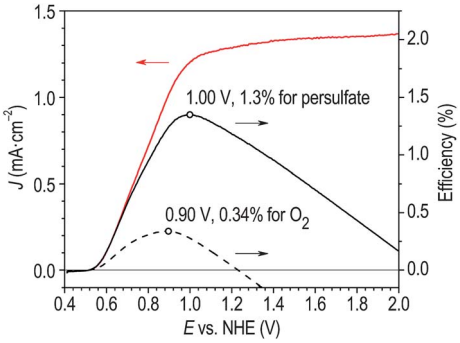

Fig. 7 Current density–potential (red) and efficiency–potential (black) behavior of WO_3 photoanodes in 1.0 M H_2SO_4. The apparent efficiencies were evaluated assuming that $S_2O_8^{2-}$(aq) (solid) or O_2(g) (dashed) was the photoanodic product. In each case, the maximum apparent efficiency is indicated at the corresponding potential.

Implications for other metal oxide photoanodes

In an analogous fashion to the photoelectrochemical behavior of WO_3 photoanodes in 1.0 M H_2SO_4 reported herein, an illuminated single-crystalline TiO_2 electrode in contact with several 2 M $(NH_4)_2SO_4$–H_2SO_4 electrolytes has been reported to produce $S_2O_8^{2-}$(aq) with η = 0.25–0.32, but no H_2O_2 was detected.[44] This behavior suggests that the initial oxidation product at TiO_2 in sulfate solutions, under acidic and near-neutral conditions, is also persulfate, as opposed to hydroxyl radical. The low $\eta(O_2)$ measured for TiO_2/H_2SO_4(aq) contacts[6] is not attributable to the formation and accumulation of H_2O_2. By extension, other metal oxide (*e.g.*, titanates and tantalates) photoanodes operating in acidic solutions of HCl or H_2SO_4 may well also predominantly produce Cl_2(g) or $S_2O_8^{2-}$(aq), respectively, as opposed to O_2(g) or H_2O_2, as primary or secondary oxidation products.

5. Conclusions

The anodic reactions at illuminated WO_3 thin films in contact with 1.0 M HCl, H_2SO_4, and $HClO_4$ were quantitatively analyzed from three perspectives: the *J*–*E* characteristics were monitored by voltammetry, the yield of dissolved O_2 was monitored by fluorescence quenching, and the yields of $S_2O_8^{2-}$(aq) and H_2O_2 were monitored using colorimetry. For all three of these acidic aqueous electrolytes, oxidation of the respective acid anion, rather than water oxidation, was the predominant process at WO_3 photoanodes. Homogeneous O_2(g) evolution from the electrolyte solution, a secondary reaction that

was not directly probed by measurement of the photoelectrochemical behavior of the anode, occurred in pure 1.0 M $HClO_4$, as well as in 1.0 M H_2SO_4 that contained Ag^+(aq) as a catalyst. In 1.0 M $HClO_4$, a hole scavenger, CPO, blocked the oxidation of ClO_4^-(aq) or water at WO_3 photoanodes, but had no effect on the electrocatalytic oxidation of water effected by RuO_2 in the dark. This rule of "anion priority" can be extended to the photoanodic oxidation of OH^-(aq) in strongly alkaline solutions, and may well apply to other metal oxide photoanodes operating in acidic or near-neutral aqueous electrolytes.

6. Acknowledgements

We acknowldge the National Science Foundation (NSF) Powering the Planet Center for Chemical Innovation (CCI-Solar), Grants CHE-0802907 and CHE-0947829, and the Molecular Materials Research Center of the Beckman Institute at the California Institute of Technology, for support. QM also acknowledges the NSF for support as a CCI-Solar Postdoctoral Fellow.

7. References

1 P. J. Boddy, *J. Electrochem. Soc.*, 1968, **115**, 199–203.
2 A. Fujishima and K. Honda, *Bull. Chem. Soc. Jpn.*, 1971, **44**, 1148–1150.
3 A. Fujishima and K. Honda, *Nature*, 1972, **238**, 37–38.
4 J. Keeney, D. H. Weinstein and G. M. Haas, *Nature*, 1975, **253**, 719–720.
5 A. J. Nozik, *Nature*, 1975, **257**, 383–386.
6 M. S. Wrighton, D. S. Ginley, P. T. Wolczanski, A. B. Ellis, D. L. Morse and A. Linz, *Proc. Natl. Acad. Sci. U. S. A.*, 1975, **72**, 1518–1522.
7 H. H. Kung, H. S. Jarrett, A. W. Sleight and A. Ferretti, *J. Appl. Phys.*, 1977, **48**, 2463–2469.
8 K. L. Hardee and A. J. Bard, *J. Electrochem. Soc.*, 1976, **123**, 1024–1026.
9 R. K. Quinn, R. D. Nasby and R. J. Baughman, *Mater. Res. Bull.*, 1976, **11**, 1011–1017.
10 A. Kay, I. Cesar and M. Grätzel, *J. Am. Chem. Soc.*, 2006, **128**, 15714–15721.
11 A. J. Cowan, C. J. Barnett, S. R. Pendlebury, M. Barroso, K. Sivula, M. Grätzel, J. R. Durrant and D. R. Klug, *J. Am. Chem. Soc.*, 2011, **133**, 10134–10140.
12 A. J. Nozik, *Annu. Rev. Phys. Chem.*, 1978, **29**, 189–222.
13 A. J. Nozik and R. Memming, *J. Phys. Chem.*, 1996, **100**, 13061–13078.
14 P. M. Woodward, H. Mizoguchi, Y. I. Kim and M. W. Stoltzfus, The electronic structure of metal oxides, in *Metal oxides: Chemistry and applications*, ed. J. L. G. Fierro, Taylor & Francis, Boca Raton, FL, 2006, pp. 133–193.
15 W. A. Gerrard, *J. Electroanal. Chem.*, 1978, **86**, 421–424.
16 M. A. Butler, R. D. Nasby and R. K. Quinn, *Solid State Commun.*, 1976, **19**, 1011–1014.
17 G. Hodes, D. Cahen and J. Manassen, *Nature*, 1976, **260**, 312–313.
18 W. Gissler and R. Memming, *J. Electrochem. Soc.*, 1977, **124**, 1710–1714.
19 H. L. Wang, T. Lindgren, J. J. He, A. Hagfeldt and S. E. Lindquist, *J. Phys. Chem. B*, 2000, **104**, 5686–5696.
20 C. Santato, M. Ulmann and J. Augustynski, *J. Phys. Chem. B*, 2001, **105**, 936–940.
21 F. Amano, D. Li and B. Ohtani, *Chem. Commun.*, 2010, **46**, 2769–2771.
22 R. Liu, Y. J. Lin, L. Y. Chou, S. W. Sheehan, W. S. He, F. Zhang, H. J. M. Hou and D. W. Wang, *Angew. Chem., Int. Ed.*, 2011, **50**, 499–502.
23 F. M. Pesci, A. J. Cowan, B. D. Alexander, J. R. Durrant and D. R. Klug, *J. Phys. Chem. Lett.*, 2011, **2**, 1900–1903.
24 J. A. Seabold and K. S. Choi, *Chem. Mater.*, 2011, **23**, 1105–1112.
25 T. Iwai, *J. Phys. Soc. Jpn.*, 1960, **15**, 1596–1600.
26 J. M. Berak and M. J. Sienko, *J. Solid State Chem.*, 1970, **2**, 109–133.
27 R. G. Breckenridge and W. R. Hosler, *Phys. Rev.*, 1953, **91**, 793–802.
28 R. Gomez, D. Monllor-Satoca, L. Borja, A. Rodes and P. Salvador, *ChemPhysChem*, 2006, **7**, 2540–2551.
29 A. Valdes and G. J. Kroes, *J. Chem. Phys.*, 2009, **130**, 114701.
30 E. A. Meulenkamp, *J. Electrochem. Soc.*, 1997, **144**, 1664–1671.
31 E. Narita, F. Lawson and K. N. Han, *Hydrometallurgy*, 1983, **10**, 21–37.
32 L. D. Burke, O. J. Murphy, J. F. Oneill and S. Venkatesan, *J. Chem. Soc., Faraday Trans. 1*, 1977, **73**, 1659–1671.
33 B. O. Loopstra and P. Boldrini, *Acta Crystallogr.*, 1966, **21**, 158–162.
34 C. Santato, M. Odziemkowski, M. Ulmann and J. Augustynski, *J. Am. Chem. Soc.*, 2001, **123**, 10639–10649.
35 J. Hanamura, K. Kobayashi, K. Kano and T. Kubota, *Chem. Pharm. Bull.*, 1983, **31**, 1357–1361.
36 H. Miyazaki, M. Yamakawa and T. Kubota, *Bull. Chem. Soc. Jpn.*, 1972, **45**, 780–785.
37 H. Jakob, S. Leininger, T. Lehmann, S. Jacobi and S. Gutewort, Peroxo compounds, inorganic, in *Ullmann's encyclopedia of industrial chemistry*, 6th edn, ed. M. Bohnet, Wiley-VCH, Weinheim, 2003.
38 L. Zhang, F. Yan, Y. N. Wang, X. J. Guo and P. Zhang, *Inorg. Mater.*, 2006, **42**, 1379–1387.
39 A. H. Maki and D. H. Geske, *J. Chem. Phys.*, 1959, **30**, 1356–1357.
40 I. V. Shimonis, *Elektrokhim.*, 1973, **9**, 1787–1789.
41 N. S. Lewis, *J. Electrochem. Soc.*, 1984, **131**, 2496–2503.
42 J.-P. Jolivet, M. Henry and J. Livage, *Metal oxide chemistry and synthesis: From solution to solid state*, John Wiley, Chichester; New York, 2000.
43 D. M. Yost, *J. Am. Chem. Soc.*, 1926, **48**, 152–164.
44 K. Kohayakawa, T. Yamabe, A. Fujishima and K. Honda, *Nippon Kagaku Kaishi*, 1978, 1351–1356.

